ACS Catalysis

Research Article

pubs.acs.org/acscatalysis

Design of Hierarchical Zeolite Catalysts for the Manufacture of Polyurethane Intermediates

Tobias C. Keller,[†] Jürgen Arras,[§] Stefan Wershofen,[§] and Javier Pérez-Ramírez*,[†]

[†]Institute for Chemical and Bioengineering, Department of Chemistry and Applied Biosciences, ETH Zurich, Vladimir-Prelog-Weg 1, CH-8093, Zurich, Switzerland

[§]Bayer MaterialScience AG, D-41538 Dormagen, Germany

Supporting Information

ABSTRACT: This study undertakes the design of hierarchically structured zeolites for the synthesis of methylenedianiline (MDA) mixtures via the liquid-phase condensation of aniline with formaldehyde. Affordable acid and base treatments enabled the controlled generation of an auxiliary network of intracrystalline mesopores within commercial zeolites of different frameworks, among which the FAU topology is identified as superior. As the micropore structure of the zeolite can be preserved, the unique shape selectivity is retained while improved mass transport in the hierarchical crystals leads to a 7-fold increased activity and a 3-fold prolonged lifetime before thermal regeneration is necessary. The linear correlation between the MDA yield and the product of the Brønsted acidity and the external surface area emphasizes the need to balance acid site and pore quality in the design of an optimal catalyst. Hierarchical USY zeolites outperform the state-of-the-art delaminated zeolites and mesoporous aluminosilicates. These results offer a viable solution for the replacement of the industrially applied homogeneous catalyst (HCl), resulting in an efficient and environmental friendly technology for the production of polyurethanes.

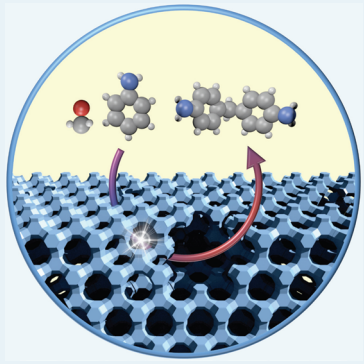

KEYWORDS: *catalyst design, hierarchical zeolite, FAU framework, methylenedianiline, polyurethanes*

1. INTRODUCTION

While zeolites are the materials of choice for gas-phase acid-catalyzed conversions, their strong Brønsted acidity and unique shape selectivity remain far less exploited in liquid-phase processes. The recent development of diverse methods to incorporate an auxiliary network of mesopores into zeolite crystals makes it possible to sidestep the underlying problem of diffusion limitations by complementing the desired zeolitic properties with an enhanced transport of bulky molecules.[1−6] Despite the reduced Brønsted acidity and microporosity that typically accompanies the introduction of extensive mesoporosity, the hierarchical catalysts exhibit an improved performance in numerous reactions of industrial relevance.[7−11]

However, as the benefits of the auxiliary porosity have been mainly demonstrated based on the comparison of a limited number of samples,[12−14] the precise impact of possible alterations of other structural characteristics as crystallinity, mesoporosity, and acidity has been less frequently quantified.[15] The identification of structure−performance relationships is crucial for the design of zeolites and could incite their application in processes where conventional zeolite catalysts are not competitive due to transport constraints.

A relevant example of such a process is the synthesis of methylenedianiline (MDA), the precursor for the most common isocyanate used in the production of polyurethanes (15.3 Mt a^{-1} in 2012).[16] MDA is industrially synthesized from the condensate of aniline and formaldehyde (called aminal) via a series of rearrangements catalyzed by HCl (Scheme 1).[17] However, as it is impossible to separate the catalyst by simple methods as distillation, the acidic solutions must be neutralized with expensive soda lye, thereby preventing catalyst reutilization, and generating problematic brine waste contaminated with chloroamine pollutants. Additionally, the necessity of corrosion-resistant equipment such as glass-lined reactors severely increases the capital cost of a plant compared to a potential heterogeneous system.[18] In spite of these economic and environmental drawbacks, the replacement of HCl has not been accomplished. As the composition of an MDA mixture has direct consequences on the quality of the obtained polyurethanes, a heterogeneous catalyst needs to fulfill the specifications of the commercially established products. Two of the dominating aspects are the achievement of a high ratio of 4,4′-MDA:2,4′-MDA (herein referred to as the "isomer ratio") and a substantial oligomeric fraction (>20%), which ensure a high melting point, flame resistance, and mechanical stability of the resulting polyurethanes due to long polymer chains and extensive cross-linking.

The first solid acids investigated were sulfonated resins,[19] natural clays,[20] and amorphous silica−aluminas (ASA).[21] Although ASA provided acceptable activity, they yielded undesirably low isomer ratios. In contrast, the defined confinement of Brønsted acid sites in zeolite micropores

Received: November 8, 2014
Revised: December 15, 2014
Published: December 15, 2014

DOI: 10.1021/cs5017694
ACS Catal. 2015, 5, 734−743

Scheme 1. Reaction Network for the Synthesis of MDA Mixtures[a]

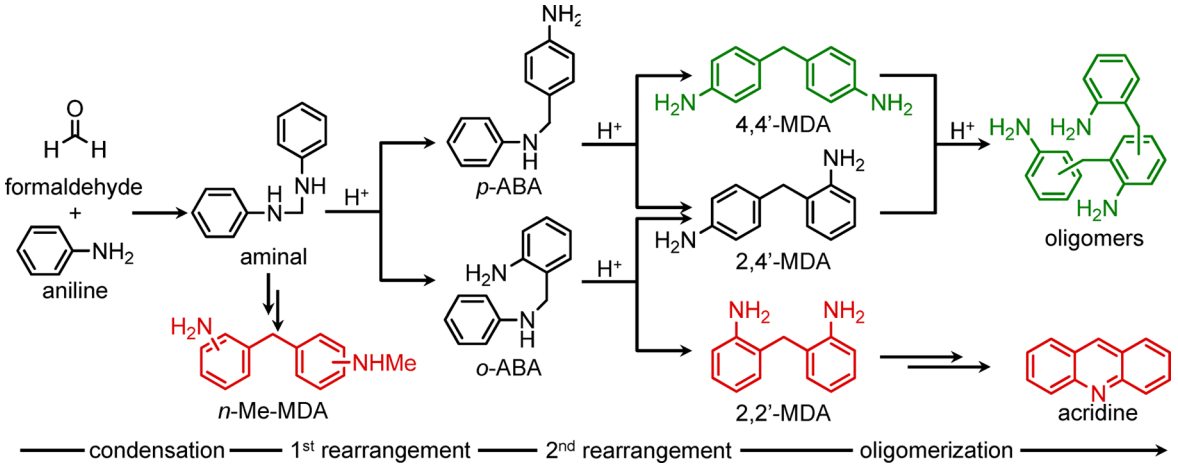

[a]Desired products are colored green and undesired by-products are colored red. The isomer ratio used along the manuscript refers to the molar ratio of 4,4′-MDA to 2,4′-MDA.

often favors the formation of one isomer over the other, which can result in an increased isomer ratio.[22−25] However, the small size of the channels dramatically slows down mass transport, which results in a severe underutilization of the active sites in the zeolite crystals. Accordingly, efforts have focused on enhancing the active site accessibility through the preparation of hierarchically structured zeolites by using two different approaches. As depicted on the left side of Scheme 2, Corma et al.[26,27] elegantly showed that highly active catalysts could be attained through the swelling and delamination of layered zeolite precursors (MCM-22(P), PREFER, and Nu-6(1)) into 2D-zeolites (ITQ-2, ITQ-6, and ITQ-18). However, delaminated zeolites yield a lower isomer ratio than ASA.[28] Taking a different approach depicted on the right side of Scheme 2, Salzinger et al.[29] attempted to derive hierarchical beta zeolite through base leaching and indeed found increased activity. The zeolites however evidenced a severe drop in crystallinity and microporosity due to the suboptimal treatment, and the eventual impact of these property alterations on the isomer ratio was not discussed. In view of the recent advancements that enabled the demetallation-based methods also for large-pore zeolites, in particular faujasites,[30] this topic deserves to be revisited.

Scheme 2. Approaches to Enhance the Micropore Accessibility and Thus the Transport of Molecules in Zeolites

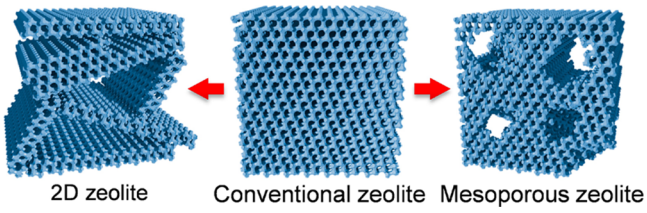

This contribution tackles the design of hierarchically structured zeolites for MDA synthesis. Affordable postsynthetic treatments are applied to introduce auxiliary mesopore networks in commercial zeolite samples. The trade-off between

Table 1. Commercial Zeolites Used in This Study and Applied Treatments to Introduce Hierarchical Porosity (H Samples)

sample	commercial name[a]	sample	treatment conditions[b]
FAU3	Zeolyst CBV300 (NH_4^+)	FAU3-H	1. 0.11 M H_4EDTA, 100 °C, 6 h, 66 $g_{zeolite}$ L^{-1} 2. 0.2 M NaOH, 65 °C, 0.5 h, 33 $g_{zeolite}$ L^{-1} 3. 0.11 M Na_2H_2EDTA, 100 °C, 6 h, 66 $g_{zeolite}$ L^{-1}
FAU6	Zeolyst CBV712 (NH_4^+)	FAU6-H	0.2 M NaOH, 65 °C, 0.5 h, 33 $g_{zeolite}$ L^{-1}
FAU15	Zeolyst CBV720 (H^+)	FAU15-H[c]	0.05−0.45 M NaOH, 0.2 M TPABr, 65 °C, 0.5 h, 33 $g_{zeolite}$ L^{-1}
		FAU15-ex	0.2 M NaOH, 65 °C, 0.5 h, 33 $g_{zeolite}$ L^{-1}
FAU30	Zeolyst CBV760 (H^+)	FAU30-H	0.15 M NaOH, 0.2 M TPABr, 65 °C, 0.5 h, 33 $g_{zeolite}$ L^{-1}
FAU40	Zeolyst CBV780 (H^+)	FAU40-H	0.05 M NaOH, 0.2 M TPABr, 65 °C, 0.5 h, 33 $g_{zeolite}$ L^{-1}
FAU385	Tosoh HSZ-390HUA (H^+)	FAU385-H	0.2 M NaOH, 0.2 M TPABr, 65 °C, 0.5 h, 33 $g_{zeolite}$ L^{-1}
BEA20	Tosoh HSZ-940HOA (H^+)	BEA20-H	0.15 M NaOH, 0.2 M TPABr, 65 °C, 0.5 h, 33 $g_{zeolite}$ L^{-1}
		BEA20-ex	0.15 M NaOH, 65 °C, 0.5 h, 33 $g_{zeolite}$ L^{-1}
MFI40	Zeolyst CBV5524G (NH_4^+)	MFI40-H	0.2 M NaOH, 65 °C, 0.5 h, 33 $g_{zeolite}$ L^{-1}
MOR10	Zeolyst CBV21A (NH_4^+)	MOR10-H	1. 3 M HNO_3, 100 °C, 1 h, 100 $g_{zeolite}$ L^{-1} 2. 0.15 M NaOH, 65 °C, 0.5 h, 33 $g_{zeolite}$ L^{-1}
HEU5	KMI Clinoptilolite (Na^+)	HEU5-H	1. Four repetitions of 1 M HCl, 100 °C, 4 h, 67 $g_{zeolite}$ L^{-1} 2. 0.2 M NaOH, 65 °C, 0.5 h, 33 $g_{zeolite}$ L^{-1}

[a]The countercation in the as-received zeolites is between brackets. [b]The numbers 1, 2, and 3 denote a sequence of treatments. [c]The sample denoted FAU15-H along the manuscript was prepared using c_{NaOH} = 0.3 M.

DOI: 10.1021/cs5017694
ACS Catal. 2015, 5, 734−743

the generation of mesopores and the gradual loss in zeolitic properties such as acidity and crystallinity is analyzed in depth. With this knowledge, the combined effects of framework topology, mesoporosity, and acidity on the catalytic activity, the isomer distribution, the oligomer selectivity, and the resistance to fouling are quantified. Benchmarking with delaminated zeolite and amorphous silica–alumina catalysts identifies hierarchical USY zeolites as the new state-of-the-art catalyst for the production of polyurethane precursors, opening a promising opportunity for the replacement of the industrially established HCl catalyst.

2. EXPERIMENTAL SECTION

2.1. Catalyst Preparation. Table 1 lists the commercial zeolites used in this study. The sample notation along the manuscript includes the framework code and the nominal Si/Al ratio, followed by the codes "C" and "H" to denote conventional (as-received) and hierarchical samples, respectively. The introduction of mesoporosity in the as-received zeolites was attained by alkaline treatment, or a combination of acid and alkaline treatments, as specified in Table 1. These protocols and specific conditions were rationalized elsewhere.[30,31] Typically, hierarchical zeolites were obtained by suspending the as-received zeolite (3.3 g) in an aqueous solution (100 cm^3) containing 0.05–0.5 M NaOH and 0–0.2 M tetrapropylammonium bromide (TPABr) at 65 °C for 30 min. All the zeolites were characterized and tested in the protonic form, which was obtained, whenever necessary, by applying three consecutive exchanges in aqueous 0.1 M NH_4NO_3 with a solid-to-liquid ratio of 10 g L^{-1} at room temperature for 8 h, followed by calcination in static air at 550 °C (heating rate = 5 °C min^{-1}) for 5 h.

ZSM-22(P), the layered precursor for ITQ-2, was prepared according to the work of Corma et al.[32] Specifically, $NaAlO_2$ (1.84 g) and NaOH (1.2 g) were dissolved in H_2O (248.4 g). Hexamethylenimine (15.22 g) was added and the solution stirred thoroughly before fumed silica (18.46 g) was added portionwise. The obtained gel was transferred into a Teflon-lined autoclave and incubated under rotation at 60 rpm and 150 °C for 7 days. The obtained solid was filtered off and washed with deionized water. The protocol to delaminate MCM-22(P) into ITQ-2 was adapted from the work of Corma et al.[26] MCM-22(P) (5.4 g) was suspended in water (99.5 g), tetrapropylammonium hydroxide solution (20 wt %, 66.5 g), and hexadecyltrimethylammonium bromide (CTAB, 7.67 g) at 80 °C for 16 h and introduced into an ultrasonic bath at 50 °C for 1 h. Through addition of 1 M HCl, the pH was lowered to 2 and the solution filtered off. The resulting solid was dried in static air at 100 °C and calcined in portions of 2 g in flowing air (60 cm^3 min^{-1}) at 550 °C (heating rate = 2 °C min^{-1}) for 8 h. Finally, ITQ-2 was converted into the protonic form following the same procedure described above. MCM-22-C was obtained by calcination of MCM-22(P) under the conditions stated above. For the synthesis of MCM-41, sodium aluminate (0.612 g) and CTAB (12 g) were dissolved in water (600 cm^3). NH_3 (25 wt % in water, 50 cm^3) were introduced, followed by dropwise addition of tetraethyl orthosilicate (50 cm^3). The slurry was then stirred for 1 h at room temperature, filtered, washed with deionized water, dried, and calcined in portions of 2 g at 550 °C (heating rate =1 °C min^{-1}) for 8 h. Amorphous silica–alumina (ASA) with a molar Si/Al ratio of 5.6 was purchased from Sigma-Aldrich (silica–alumina catalyst support, grade 135) and calcined at 550 °C (heating rate = 5 °C min^{-1}) for 5 h.

2.2. Catalyst Characterization. Powder X-ray diffraction (XRD) was measured in a PANalytical X'Pert PRO-MPD diffractometer with Bragg–Brentano geometry using Ni-filtered Cu Kα radiation (λ = 0.1541 nm). The patterns were recorded in the 2θ range of 5–70° with an angular step size of 0.05° and a counting time of 8 s per step. The relative crystallinity of the samples was determined following ASTM standards D3906 (FAU) and D5758 (MFI). For MOR, BEA, and HEU samples, the relative intensity of the reflection at 22.5° 2θ was considered. The amount of Si and Al in the solids was determined by inductively coupled plasma optical emission spectroscopy (ICP-OES) using a Horiba Ultima 2 instrument equipped with photomultiplier tube detection. Samples (20 mg) were dissolved in 3 M NaOH (10 mL) at 65 °C, diluted with deionized water (90 mL), and measured with a 5-point calibration curve. Nitrogen sorption at −196 °C was carried out in a Micromeritics TriStar II instrument. Prior to the measurement, the samples were evacuated at 300 °C for 3 h. The total surface area was determined by the BET equation, the *t*-plot method was used to discriminate between micro- and mesoporosity. The pore size was determined by application of the BJH model to the adsorption branch of the isotherm. Scanning electron microscopy (SEM) and transmission electron microscopy (TEM) images were performed on Zeiss Gemini 1530 FEG (5 kV) and FEI Tecnai F30 (300 kV) microscopes, respectively. Temperature-programmed desorption of ammonia (NH_3-TPD) was carried out in a Thermo TPDRO 1100 unit. The zeolite (0.1 g) was pretreated at 550 °C in He flow (30 cm^3 min^{-1}) for 3 h. Afterward, 10 vol % of NH_3 in He (30 cm^3 min^{-1}) was adsorbed three times at 200 °C for 30 min, followed by He purging at the same temperature for 60 min. The desorption of ammonia was monitored with a thermal conductivity detector (TCD) in the range of 200–700 °C using a ramp of 10 °C min^{-1}. Fourier transform infrared spectroscopy (FTIR) of adsorbed pyridine was conducted in a Bruker IFS 66 spectrometer by coaddition of 32 scans in the range of 650–4000 cm^{-1} with an optical resolution of 4 cm^{-1}. The powdered zeolites were pressed into self-supporting wafers of ca. 1 cm^2 and degassed under vacuum (10^{-3} mbar) at 420 °C for 4 h, followed by pyridine adsorption at room temperature. Gaseous and weakly adsorbed molecules were subsequently removed by evacuation at 200 °C for 30 min.

2.3. Catalyst Testing. To prepare the condensate of aniline and formaldehyde ("aminal solution"), aniline (150 g) was heated to 80 °C under nitrogen atmosphere. Then, formaldehyde solution (37 wt %, 134 g) and additional aniline (according to the desired A/F ratio) were added dropwise during 20 min. After stirring for additional 10 min, the solution was allowed to settle and the aqueous phase removed using a separation funnel. High-throughput catalytic tests in batch mode were carried out in an AMTEC SPR16 system equipped with 16 stainless steel 15 cm^3 reactors. Each reactor was charged with the catalyst (m_{cat} = 0.1–1 g) and purged three times with nitrogen. Then, the aminal solution (4.9 g) was introduced. The suspension was heated to the reaction temperature (50–170 °C) with a heating rate of 10 °C min^{-1}, and left to react for 1–4 h under autogenous pressure with magnetic stirring at 500 rpm. After cooling the reactor to room temperature, liquid samples were taken, diluted in *n*-ethyldiisopropylamine, and analyzed off-line by high performance liquid chromatography (HPLC) using an Agilent 1100

DOI: 10.1021/cs5017694
ACS Catal. 2015, 5, 734–743

Table 2. Characterization Data of the Catalysts

sample	Si/Al[a] [mol mol^{-1}]	V_{micro}[b] [cm^3 g^{-1}]	V_{pore} [cm^3 g^{-1}]	S_{meso}[b] [m^2 g^{-1}]	S_{BET}[c] [m^2 g^{-1}]	crystallinity[d] [%]	$c_{Brønsted}$[e] [μmol g^{-1}]	c_{Lewis}[e] [μmol g^{-1}]
FAU3-C	2.5	0.36	0.38	24	718	100	584	207
FAU3-H	4.0	0.22	0.64	212	635	51	302	171
FAU6-C	5.9	0.28	0.45	120	666	100	262	108
FAU6-H	5.0	0.27	0.71	346	862	54	176	182
FAU15-C	15.9	0.32	0.54	144	760	100	220	69
FAU15-H	11.1	0.26	1.00	533	1030	64	125	111
FAU15-ex	11.2	0.0	0.69	576	576	0	31	72
FAU30-C	29.9	0.32	0.56	171	797	100	151	37
FAU30-H	18.5	0.25	0.96	418	907	76	141	99
FAU40-C	47.8	0.26	0.52	226	734	100	52	8
FAU40-H	39.1	0.15	0.75	454	737	33	59	32
FAU385-C	385	0.29	0.53	108	668	100	10	0
FAU385-H		0.27	0.76	253	775	55	9	4
BEA20-C	21.3	0.21	0.29	117	510	100	143	79
BEA20-H	13.8	0.19	0.44	297	615	61	109	102
BEA20-ex		0.07	0.42	470	615	16	66	42
MFI40-C	39	0.21	0.27	31	433	100	174	19
MFI40-H	25	0.12	0.54	278	511	72	147	78
MOR10-C	10	0.14	0.25	115	392	100	149	25
MOR10-H		0.21	0.40	132	540	79	226	90
HEU5-C	5.2	0.09	0.15	35	198	100	18	4
HEU5-H		0.09	0.35	70	251	96	17	5
ITQ-2	15.6	0.06	0.88	637	715		159	375
MCM-41	30.5	0	0.91	1386	1386		26	41
ASA	5.6	0	0.78	593	593		34	69
MCM-22-C		0.18	0.48	122	458			

[a]ICP-OES. [b]*t*-plot method. [c]BET method. [d]XRD. [e]IR of adsorbed pyridine.

chromatograph with a methanol/water/aniline mixture as eluent and a Waters XTerra MS C18 column. The reproducibility of the catalytic tests was ensured by carrying out 16 catalytic tests under identical conditions (Table S1). The relative standard deviation (%RSD) was found to be <1.5% for 4,4′-MDA and 2,4′-MDA, and <5% for 2,4′-MDA, oligomers, and *n*-Me-MDA. Reusability experiments without calcination were carried out in a 250 cm^3 Parr autoclave by reacting aminal (176 g) over 9 g of catalyst at 140 °C for 4 h. After the reaction, the product solution was removed through a metal frit filter, and the catalyst washed 3 times with aniline (200 cm^3) at 140 °C for 1 h, before fresh aminal was added. Liquid samples were characterized as stated above.

3. RESULTS AND DISCUSSION

The preparation and in-depth characterization of the catalysts is described in section 3.1. Section 3.2 elaborates the importance of zeolite framework and composition on the MDA synthesis, while in section 3.3 a structure-performance relationship for USY zeolites is established. Finally, section 3.4 summarizes further opportunities arising from hierarchical zeolites and their implications on industrial MDA production.

3.1. Properties of the Catalysts. Commercially obtained zeolites of varying framework and composition have been investigated in conventional and hierarchical form. The catalysts were characterized in protonic form by N_2 sorption, XRD, elemental analysis, and pyridine-IR. The results are summarized in Table 2, and representative nitrogen isotherms, BJH pore-size distributions, and X-ray diffractograms are provided in the Supporting Information in Figures S1, S2, and S3, respectively. For all investigated zeolites, hierarchical analogues were derived through a combination of acid and base treatments. The efficiency of the treatments to introduce mesopores strongly depends on the zeolites framework, composition, and porosity. Samples combining highly accessible frameworks with an intermediate Si/Al ratio provide ideal preconditions, while the demetallation of Al-rich or severely Al-deficient zeolites is more difficult. External surface areas (S_{meso}) of up to 550 m^2 g^{-1} were attained for three-dimensional frameworks such as FAU, BEA, and MFI, whereas frameworks of lower dimensionality (HEU and MOR) were less susceptible to the treatments ($S_{meso} \approx 100$ m^2 g^{-1}). The generation of mesoporosity is often accompanied by adverse effects such as a reduction in micropore volume, acidity, and crystallinity, which need to be moderated, thus limiting the attainable mesoporosity. The optimization of the treatments has been rationalized in previous contributions[30,31] and is thus not further discussed herein. Typically, an increase in external surface area by a factor of 3−5 could be attained, which was accompanied by a 20−40% reduction in crystallinity and Brønsted acidity, while the concentration of Lewis acid sites increased. As an exception, the micropore volume and the Brønsted acidity of the investigated mordenite sample (MOR10) were substantially increased after the treatments. This effect likely results from the removal of nonframework material that blocked the access to the one-dimensional channels and thus significantly reduced the micropore volume, or through selective dissolution of noncrystalline domains.

Due to the promising shape selectivity of the FAU framework (vide infra), zeolite Y (FAU3) and USY (FAU6-385) were studied in more detail. These commercial USY catalysts are typically prepared by sequential steaming and acid-

DOI: 10.1021/cs5017694
ACS Catal. 2015, 5, 734−743

leaching of hydrothermally synthesized zeolite Y. With the extent of the dealumination, the external surface is increased, while both the Brønsted and the Lewis acidity are reduced. Characterization by NH_3-TPD further evidences an optimum in acid strength for samples of an intermediate Si/Al ratio such as FAU15 and FAU30 (Figure 1). This textural and compositional diversity has major consequences on the susceptibility of the FAU zeolites to acid- and base treatments. Accordingly, the postsynthetic modification strategy to introduce an auxiliary mesopore network into FAU zeolites has to be adapted based on the composition. For the Al-rich FAU3 zeolite, a liquid-phase dealumination treatment with H_4EDTA is necessary to enable mesopore formation by a subsequent alkaline treatment. In contrast, the FAU6 zeolite can be directly subjected to an alkaline treatment (Figure S4), and for higher Si/Al ratios the application of pore-directing agents is required to prevent an excessive dissolution and amorphization.

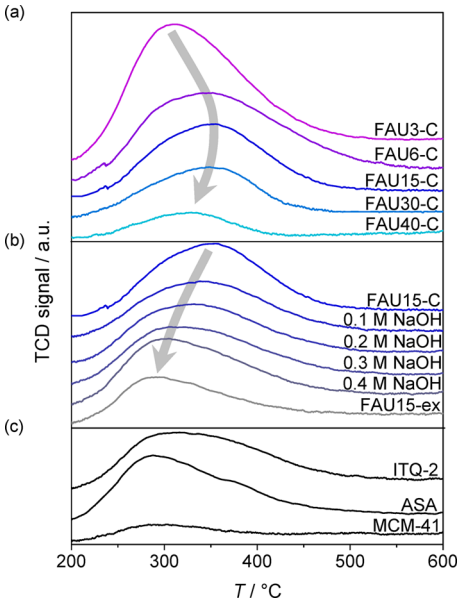

Figure 1. NH_3-TPD profiles of (a) the conventional FAU-type zeolites, (b) the FAU15 samples base-treated at varying concentrations of NaOH in presence or absence of pore-directing agents (see Table 1), and (c) the reference aluminosilicate catalysts investigated in this study.

The Al-rich zeolites exhibited the highest relative differences for both mesoporosity and acidity, with an up to 9-fold increase in external surface accompanied by a 50% drop in acidity. In contrast, for zeolites with lower Al contents S_{meso} could only be tripled, but the acidity was preserved at a much higher level. With 533 $m^2\ g^{-1}$, the highest external surface area was achieved for the FAU15-H zeolite, yielding a micro- and mesoporous material with preserved crystal morphology (Figure 2a). Further, the ^{27}Al MAS NMR spectra evidence only minor changes in the chemical environment of aluminum (Figure S5). For this zeolite, the evolution of material properties with the alkalinity of the applied solution was studied in depth (Figure 3). The base leaching leads to a steady increase in pore volume (V_{pore}), while the Si/Al ratio is reduced due to the preferential removal of silicon. At low concentrations, mesopores in the size of d_p = 3−4 nm are developed (Figure S2). For samples treated under harsher conditions, a secondary mesopore system of d_p = 10−15 nm is observed. The external surface area was found to increase linearly with the applied sodium hydroxide concentration until a maximum is achieved at c_{NaOH} = 0.35 M. While the zeolite framework appears to be initially unaffected by the dissolution, a gradual reduction of the micropore volume and

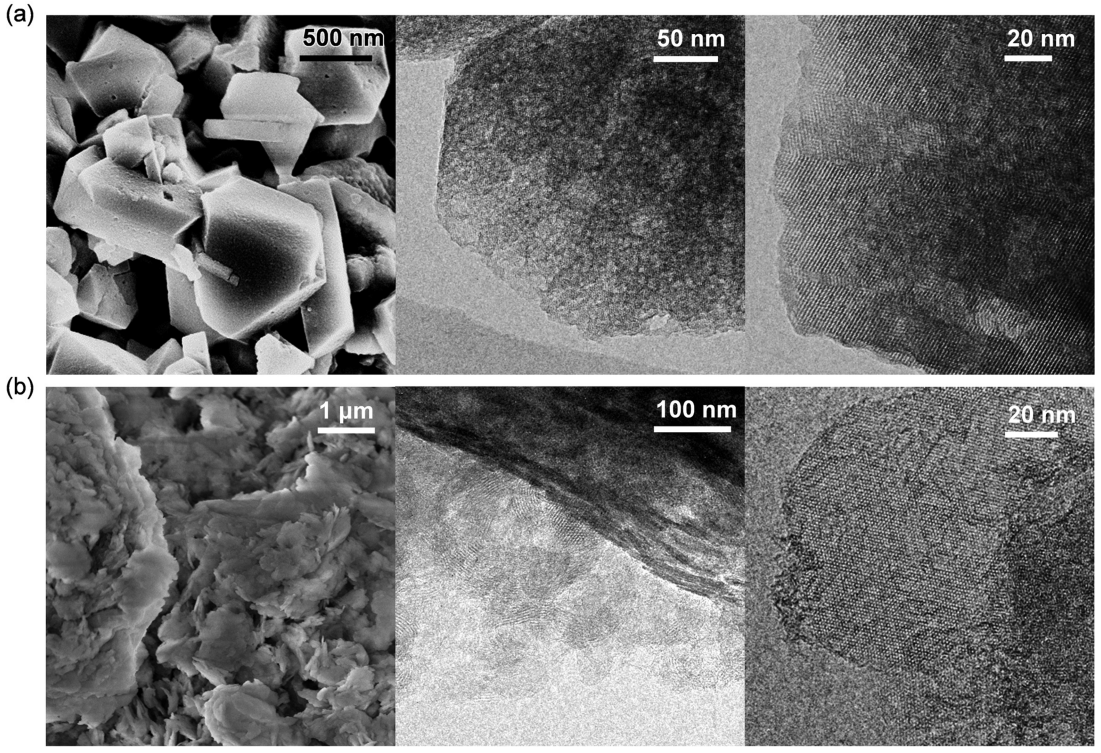

Figure 2. Scanning (left) and transmission (middle and right) electron micrographs of (a) FAU15-H and (b) ITQ-2 zeolites.

DOI: 10.1021/cs5017694
ACS Catal. 2015, 5, 734−743

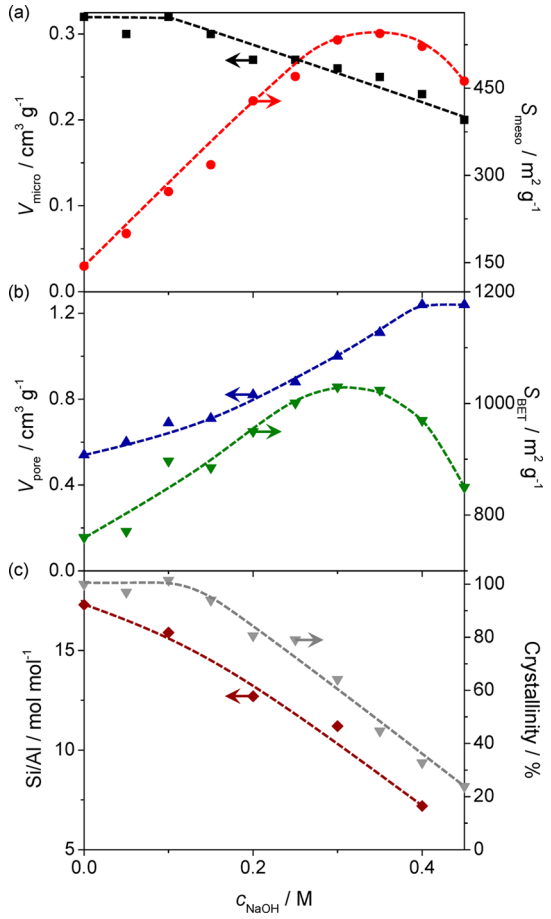

Figure 3. (a) Micropore volume and mesopore surface area, (b) total pore volume and BET surface area, and (c) molar Si/Al ratio and crystallinity of FAU15 zeolites treated in aqueous NaOH solutions of different concentrations (0.05−0.45 M) in the presence of 0.2 M TPABr at 65 °C with a solid-to-liquid ratio of 33 g L^{-1} for 30 min. Symbols at c_{NaOH} = 0 M represent the properties of the conventional (untreated) zeolite.

the crystallinity is observed at c_{NaOH} > 0.1 M. The concentration of Brønsted acid sites significantly drops already at low alkalinity, but stabilizes at ca. 60% of its initial value (Figure 4). In contrast, the Lewis acidity exhibits an exponential

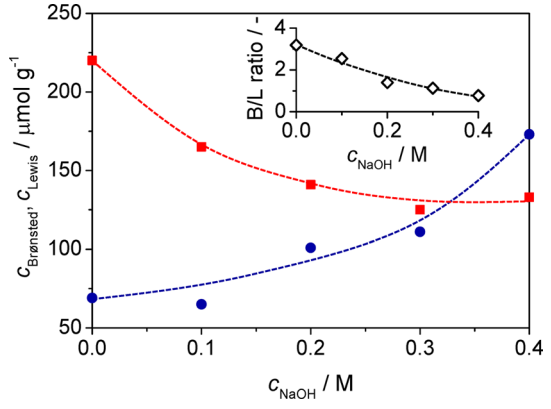

Figure 4. Concentration of Brønsted (squares) and Lewis (circles) acid sites in FAU15 zeolites characterized by infrared spectroscopy of adsorbed pyridine. The inset shows the ratio of Brønsted-to-Lewis sites.

growth, leading to a steadily decreasing Brønsted-to-Lewis ratio. The decrease in total acidity, as well as the reduction in acid strength are confirmed by NH_3-TPD, where a shift of the desorption maximum toward lower temperatures is observed. If FAU15 is treated in absence of a pore-directing agent (FAU15-ex), an amorphous material with an external surface area of S_{meso} = 576 m^2 g^{-1} is obtained, whose acidic properties strongly resemble the investigated ASA catalyst.

Several aluminosilicate catalysts providing mesopores with high accessibility have been investigated as reference catalysts. The hydrothermal synthesis of MCM-22(P), the layered precursor of ITQ-2, yielded a crystalline solid without side-phases (Figure S4). After swelling and delamination, ITQ-2 was successfully obtained as evidenced by N_2 sorption (Figure S1), XRD (Figure S3), and TEM (Figure 2b). Its external surface area (S_{meso} = 637 m^2 g^{-1}) slightly exceeded the maximum values obtained by desilication, indicating a high degree of delamination. While it provided the highest Lewis acidity (c_{Lewis} = 375 µmol g^{-1}) among all investigated samples, its Brønsted acidity ($c_{Brønsted}$ = 159 µmol g^{-1}) was similar to the hierarchical FAU15 samples. The synthesis of MCM-41 with a Si/Al ratio of 30 yielded an ordered mesoporous material (Figure S4) with a pore-size of 2.5 nm (Figure S2) and low acidity. In contrast, a commercial ASA with Si/Al = 5.6 only provided half the surface, but an increased acid site density. The NH_3 desorption maximum, indicative of the acid strength, was similar for the two amorphous catalysts (Figure 1). ITQ-2 provided slightly stronger acid sites, with the USY samples being the strongest acids investigated.

3.2. Selection of Framework Type and Composition.

In MDA synthesis, the zeolite framework does not only determine the obtained isomer ratio via its shape-selective properties, but the accessibility of the framework also strongly affects its catalytic activity. To quantify these effects, and to ensure the selection of an optimal framework, several commercially available zeolites were tested in the condensation of aniline with formaldehyde in their conventional and hierarchical form. The isomer ratio was mapped against the catalyst productivity for 2-ring MDA (Figure 5), where optimal samples appear in the top-right corner. Indeed, the highly accessible frameworks with a 3D network of 12MR pores (FAU, BEA) were identified as most active zeolites. Upon introduction of mesoporosity, the activity of all zeolites was consistently increased, clearly evidencing the negative impact of mass transport limitations on the catalytic activity. While the amorphous materials provided an isomer ratio of 5 under the investigated conditions, each zeolite attained a characteristic isomer ratio. This shape selectivity was retained for the hierarchical analogues of all investigated samples, strongly suggesting that the reaction still occurs in the confinement of the micropores, and that the underlying chemistry is unaffected by the postsynthetic treatments. To confirm this observation, the activation energies for the formation of 4,4′-MDA and 3-ring oligomers have been determined for the conventional and hierarchical FAU15 zeolite in the range of 50 to 110 °C using five temperature points. The activation energy for 4,4′-MDA formation is similar for the conventional ($E_{a,C}$ = 74 kJ mol^{-1}) and the hierarchical sample ($E_{a,H}$ = 80 kJ mol^{-1}). The apparent activation energy for oligomer formation was lowered through the treatment, but again no statistically significant difference was observed ($E_{a,C}$ = 145 kJ mol^{-1}, $E_{a,H}$ = 131 kJ mol^{-1}). The limited acid site accessibility prevents full utilization of the

DOI: 10.1021/cs5017694
ACS Catal. 2015, 5, 734−743

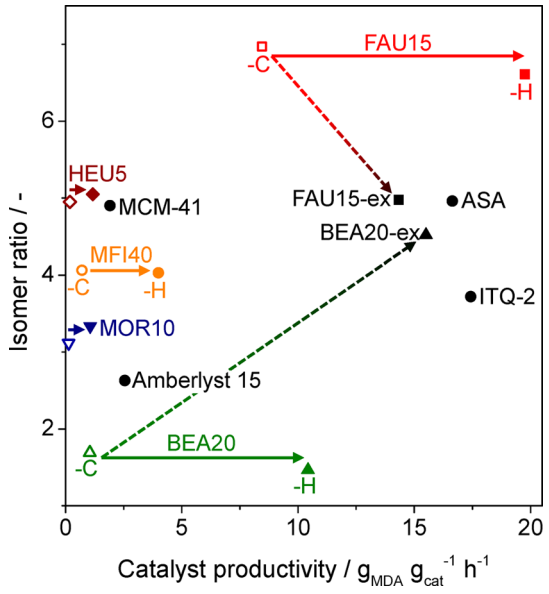

Figure 5. MDA isomer ratio versus productivity for 2-ring MDA obtained over conventional (open symbols, −C) and hierarchical (full symbols, −H) zeolites and reference catalysts (circles) (conditions: m_{cat} = 0.1 g, A/F = 3, T = 140 °C, t = 1−4 h).

zeolite already at temperatures as low as 50 °C, where hierarchical structuring results in a doubled activity.

The excellent activity and isomer distribution of FAU-type zeolite renders them a promising catalyst for further optimization. Therefore, a broad compositional range of commercial Y and USY zeolites was tested. Their catalytic activity is strongly influenced by their aluminum content (Figure 6) and displays a volcano-type behavior with an

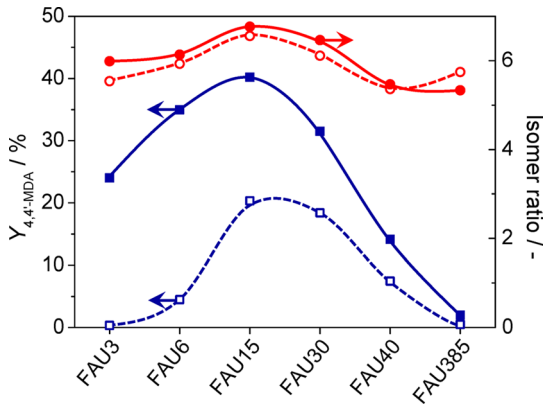

Figure 6. Yield of 4,4′-MDA (squares) and isomer ratio (circles) over conventional (open symbols) and hierarchical (full symbols) FAU zeolites (conditions: m_{cat} = 0.1 g, A/F = 3, T = 140 °C, t = 2 h).

optimum at Si/Al = 15. The underlying effect is the trade-off between accessibility and acidity: Al-rich FAU type zeolites (Si/Al = 2.5−3) such as FAU3 provide a high acidity but very low external surface areas. In contrast, high-silica USY zeolites (Si/Al > 100) such as FAU385 possess mesopores originating from steaming and acid leaching but very low acidity. Accordingly, upon hierarchical structuring, the biggest benefits could be attained for the Al-rich samples, while the activity is only marginally increased over their Al-deficient counterparts. As an example, the FAU6-C zeolite attained an MDA yield of 5% in conventional form. In hierarchical form (FAU6-H), a 7-fold increase in activity is observed, rendering it one of the most efficient catalysts in the study. The isomer ratios obtained over all FAU catalysts lie around 6 ± 0.5 and are, again, unaffected by the hierarchical structuring, confirming the predominant role of the framework for this performance indicator.

3.3. Structure−Performance Relationship. Due to its ideal combination of acidity and mesoporosity, the FAU15 zeolite offers the ideal preconditions for MDA synthesis, and through alkaline treatments, its performance can be even further increased (Figure S6). However, as a stronger treatment does not necessarily result in a better catalyst, the identification of an accurate performance descriptor that explains the catalytic activity on the basis of material properties is essential. If the MDA yield is mapped against the product of external surface area and Brønsted acidity, a linear dependence is evidenced for both the 4,4′- and the 2,4′-isomer (Figure 7). This structure-

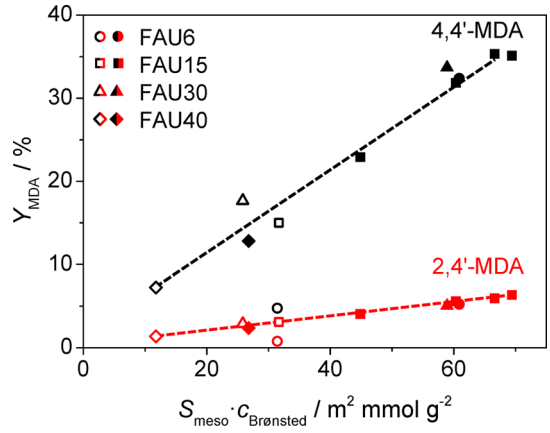

Figure 7. Correlation between the yield of 2-ring MDA isomers and the product of Brønsted acidity and mesopore surface area over conventional (open symbols) hierarchical (full symbols) USY zeolites (conditions: m_{cat} = 0.1 g, A/F = 3, T = 140 °C, t = 1 h).

performance relationship is valid also for USY zeolites of other Si/Al ratios, illustrating the necessity of both acidity and accessibility that in unison contribute to the catalytic activity. The only outlier is the FAU6-C sample, which likely exhibits occluded mesopores formed during the steam treatment that result in an overestimation of the catalytic performance.[33,34] Accordingly, a term quantifying the mesopore connectivity, as recently developed by positron annihilation lifetime spectroscopy, could further improve the quality of the estimation.[35] As long as the crystalline structure of the zeolite is preserved, the obtained results can be extrapolated to other methods to synthesize mesoporous zeolites. As an example, ITQ-2 provides similar acidity and mesoporosity as the hierarchical USY zeolites, and indeed also performs on the same level of activity. However, the superior isomer ratio obtained over hierarchical USY zeolites clearly underlines their status as new state-of-the-art catalyst for MDA synthesis. In contrast, if the treatments cause severe damage to the crystalline framework, the related shape selectivity is lost. This could be demonstrated for both the FAU15-ex and the BEA20-ex samples, which were desilicated in absence of pore-directing agents, similar to the approach taken by Salzinger et al.[29] Both samples exhibit a substantially reduced crystallinity, and while the formation of mesopores leads to an increased activity, the obtained isomer

DOI: 10.1021/cs5017694
ACS Catal. 2015, 5, 734−743

rations are in line with investigated amorphous silica−alumina samples (Figure 5).

3.4. Impact on the Industrial Process. The introduction of mesoporosity also enables to resolve further major issues that prevented an implementation of zeolites. While industrially obtained MDA mixtures contain up to 30% of oligomers in the reaction solution before workup, conventional USY catalysts did not exceed 18% even when working at a lower A/F ratio that favor the oligomer formation (Figure 8a). In contrast, the

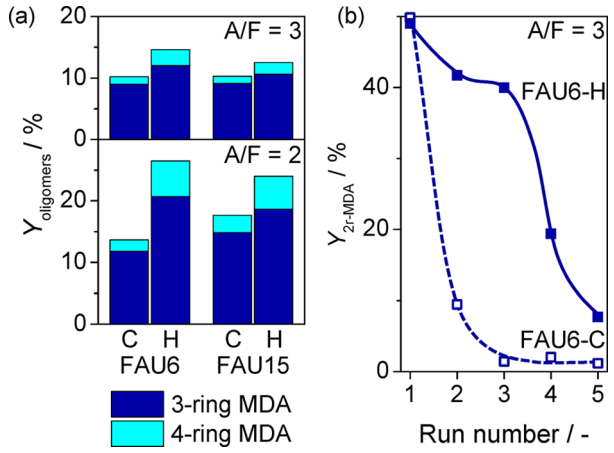

Figure 8. (a) Oligomer selectivity at full conversion obtained at different A/F ratios over conventional and hierarchical FAU6 zeolites. (b) Yield of MDA over the FAU6 samples in reusability tests without intermediate calcination (conditions: m_{cat} = 1 g, T = 140 °C, t = 4 h).

shorter diffusion pathways in mesoporous samples facilitate the transport of oligomers out of the framework. Thus, the oligomer yield is strongly increased for the hierarchical samples, in particular for the 4-ring fraction. Since pore-blocking by oligomers is the major reason for deactivation,[29] an increased lifetime of the catalyst could also be expected. Indeed, if the conventional FAU6-C catalyst is reused without calcination, ca. 80% of its initial activity is lost after one run even if the catalyst is washed with aniline at 140 °C before its reutilization (Figure 8b). Over its hierarchical counterpart, two additional runs can be carried out before its activity is reduced below 80% of its initial performance. However, as the deactivation is connected to the microporous nature of the zeolite, a thermal regeneration is ultimately still necessary. This can be achieved via a calcination at 550 °C, where the catalyst can be regenerated at least 6 times without significant loss in activity (Figure S7).

As mentioned in the Introduction (Scheme 1), byproducts such as 2,2′-MDA and *n*-Me-MDA could prevent the industrial implementation of an otherwise successful catalyst, and thus deserve being discussed. 2,2′-MDA, the thermodyamically favored MDA isomer, reacts to quinolines that ultimately lead to inacceptable coloring of the PUR plastics, and thus its contents should be kept at a minimum. *n*-Me-MDA is a disproportionation product of the aminal that is converted into a monoisocyanate during phosgenation. Therefore, it acts as a chain stopper that can dramatically reduce the average chain length of a polymer already at low concentrations. As indicated in Table S1, the FAU15-C zeolite attained an 2,2′-MDA content of 0.40 wt %, and an *n*-Me-MDA content of 0.31 wt % if aminal of an A/F = 3 is reacted over 1 g of zeolite at 140 °C. Under identical reaction conditions, its hierarchical analogue FAU15-H attained a 2,2′-MDA content of 0.44 wt % and a *n*-Me-MDA content of 0.29 wt %. The 2,2′-MDA content lies within the industrial norm and thus does not appear to be a critical issue. In contrast, the *n*-Me-MDA content should be slightly reduced, which can be achieved by optimization of the reaction conditions: The rearrangement of the aminal mixture at temperatures larger than 80 °C, as carried out in this study to obtain kinetically meaningful data favors the formation of *n*-methyl-MDA due to the high temperature at low conversion levels. In an optimized, industrial reaction protocol, a significant part of the aminal can be rearranged at low temperature in the range of 50−100 °C, before the reaction is finalized at high temperature. This is expected to lead to the required reduction in the byproduct formation. In this low-temperature regime (50−100 °C), the advantages of hierarchical zeolites over ASA catalysts become more evident, as the activity of zeolites is approximately one order of magnitue higher compared to ASA catalysts (Figure 9a). Additionally, the differences in isomer distributions become more pronounced at low temperatures (Figure 9b), further improving this key advantage of zeolite catalysts.

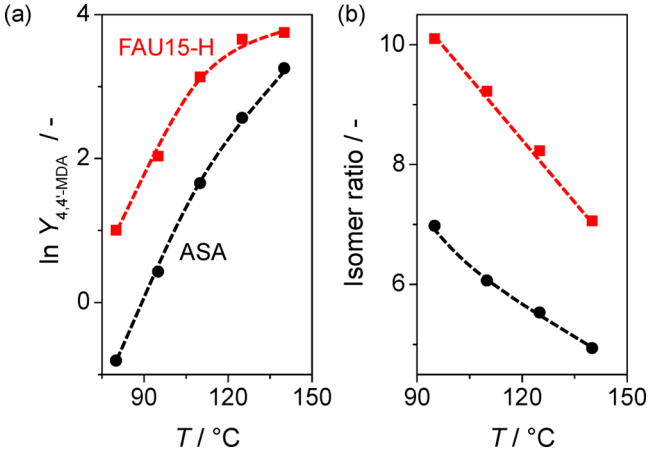

Figure 9. Influence of the reaction temperature on (a) the 4,4′-MDA yield and (b) isomer distribution obtained over FAU15-H (red) and ASA (black) catalysts (conditions: m_{cat} = 0.1 g, A/F = 3, t = 4 h).

In this study, we demonstrate how the shorter diffusion pathways enable an increased catalyst effectiveness, while the deactivation through pore-blockage by oligomer formation is delayed (Scheme 3). However, the microporous nature ultimately still leads to their deactivation. Therefore, future studies should develop a deeper understanding of the deactivation mechanism, to estimate how the lifetime of a zeolite catalyst can be further extended, i.e. through the optimization of the reaction protocol. With this input, the reactor configuration (batch or continuous) for an industrial process can be decided. Furthermore, the shape selectivity of zeolites is still poorly understood. While numerous frameworks have been tested, the number of structures with an improved shape selectivity is limited. In view of the increasing number of new zeolites, in particular considering the recently developed ADOR (assembly disassembly organization reassembly) methods,[6] the assessment and understanding of the shape selective properties holds huge potential for the further development of zeolite catalysts. As an example, Tosoh recently patented the application of EMT zeolites for MDA synthesis, claiming superior 4,4′-MDA selectivity compared to FAU-type zeolites.[36]

DOI: 10.1021/cs5017694
ACS Catal. 2015, 5, 734−743

Scheme 3. Benefits of Hierarchical Porosity in FAU Zeolites for the Synthesis of Methylenedianiline Mixtures upon the Liquid-Phase Reaction of Aniline and Formaldehyde[a]

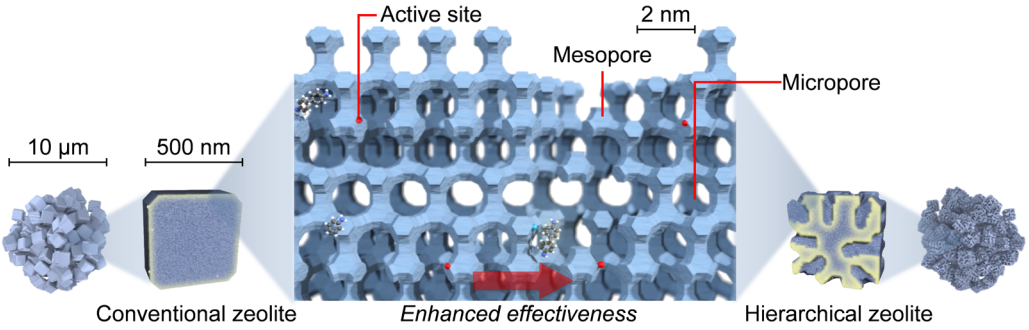

[a]The hierarchical zeolite provides preserved shape selectivity in combination with shorter diffusion pathways, leading to an enhanced catalyst effectiveness.

4. CONCLUSIONS

We showed a successful strategy to design hierarchically structured zeolite catalysts for the synthesis of methylendianiline (MDA) by the liquid-phase reaction of aniline and formaldehyde. The controlled generation of intracrystalline mesopores within commercial zeolite crystals by affordable postsynthetic treatments is highly beneficial, leading to (i) an enhanced activity, (ii) a high isomer ratio, (iii) an increased oligomer fraction, and (iv) an improved resistance to fouling. Hierarchical USY (faujasite structure) outperform all the zeolite frameworks evaluated, as well as other state-of-the-art catalysts such as delaminated zeolites and mesoporous aluminosilicates. We demonstrate that the mesoporosity, acidity, and crystallinity should be carefully balanced to attain a superior faujasite catalyst. This result paves the way for the more sustainable manufacture of polyurethanes by replacing the currently applied mineral acids (homogeneous catalysts) with environmentally benign heterogeneous alternatives.

■ ASSOCIATED CONTENT

Supporting Information

The following file is available free of charge on the ACS Publications website at DOI: 10.1021/cs5017694.

Characterization of the samples by N_2 sorption, mesopore size distributions, X-ray diffraction, and electron microscopy. Reproducibility of the catalytic tests. Catalytic data of FAU15 samples for MDA synthesis and reusability tests with intermediate calcination of FAU6-H. (PDF)

■ AUTHOR INFORMATION

Corresponding Author

*Phone: +41-44-633-7120. E-mail: jpr@chem.ethz.ch.

Notes

The authors declare no competing financial interest.

■ ACKNOWLEDGMENTS

This work was funded by ETH Zurich (Grant ETH-31 13-1), the Swiss National Science Foundation (Project 200021-134572), and the European Institute of Innovation and Technology via the Climate-KIC partnership (Dream Products). We thank Stephan Kaliga and Anna Beltzung for experimental input and Dr. Markus Dugal for fruitful discussions. Dr. Sharon Mitchell and Nina-Luisa Michels are acknowledged for TEM and SEM analyses, respectively.

■ REFERENCES

(1) Hartmann, M. *Angew. Chem., Int. Ed.* **2004**, *43*, 5880−5882.
(2) Pérez-Ramírez, J.; Christensen, C. H.; Egeblad, K.; Christensen, C. H.; Groen, J. C. *Chem. Soc. Rev.* **2008**, *37*, 2530−2542.
(3) Buurmans, I. L. C.; Ruiz-Martínez, J.; Knowles, W. V.; van der Beek, D.; Bergwerff, J. A.; Vogt, E. T. C.; Weckhuysen, B. M. *Nat. Chem.* **2011**, *3*, 862−867.
(4) Lopez-Orozco, S.; Inayat, A.; Schwab, A.; Selvam, T.; Schwieger, W. *Adv. Mater.* **2011**, *23*, 2602−2615.
(5) Serrano, D. P.; Escola, J. M.; Pizarro, P. *Chem. Soc. Rev.* **2013**, *42*, 4004−4035.
(6) Roth, W. J.; Nachtigall, P.; Morris, R. E.; Čejka, J. *Chem. Rev.* **2014**, *114*, 4807−4837.
(7) de Jong, K. P.; Zečević, J.; Friedrich, H.; de Jongh, P. E.; Bulut, M.; van Donk, S.; Kenmogne, R.; Finiels, A.; Hulea, V.; Fajula, F. *Angew. Chem., Int. Ed.* **2010**, *49*, 10074−10078.
(8) van Laak, A. N. C.; Sagala, S. L.; Zečević, J.; Friedrich, H.; de Jongh, P. E.; de Jong, K. P. *J. Catal.* **2010**, *276*, 170−180.
(9) Olsbye, U.; Svelle, S.; Bjørgen, M.; Beato, P.; Janssens, T. V. W.; Joensen, F.; Bordiga, S.; Lillerud, K. P. *Angew. Chem., Int. Ed.* **2012**, *51*, 5810−5831.
(10) Song, Y.; Hua, Z.; Zhu, Y.; Zhou, J.; Zhou, X.; Liu, Z.; Shi, J. *J. Mater. Chem.* **2012**, *22*, 3327−3329.
(11) Jo, C.; Ryoo, R.; Žilková, N.; Vitvarovác, D.; Čejka, J. *Catal. Sci. Technol.* **2013**, *3*, 2119−2129.
(12) Martens, J. A.; Verboekend, D.; Thomas, K.; Vanbutsele, G.; Gilson, J.-P.; Pérez-Ramírez, J. *ChemSusChem* **2013**, *6*, 421−425.
(13) Martínez, C.; Verboekend, D.; Pérez-Ramírez, J.; Corma, A. *Catal. Sci. Technol.* **2013**, *3*, 972−981.
(14) Sartipi, S.; Parashar, K.; Makkee, M.; Gascon, J.; Kapteijn, F. *Catal. Sci. Technol.* **2013**, *3*, 572−575.
(15) Milina, M.; Mitchell, S.; Michels, N.-L.; Kenvin, J.; Pérez Ramírez, J. *J. Catal.* **2013**, *308*, 398−407.
(16) Grunert, F. *Kunststoffe Int.* **2013**, *10*, 84−90.
(17) Wegener, G.; Brandt, M.; Duda, L.; Hofmann, J.; Klesczewski, B.; Koch, D.; Kumpf, R.-J.; Orzesek, H.; Pirkl, H.-G.; Six, C.; Steinlein, C.; Weisbeck, M. *Appl. Catal., A* **2001**, *221*, 303−335.
(18) de Angelis, A.; Ingallina, P.; Perego, C. *Ind. Eng. Chem. Res.* **2004**, *43*, 1169−1178.
(19) Merger, F.; Nestler, G., BASF AG. Process for the preparation of polyamine mixtures with a big portion of 4,4'-diamino-diphenyl methane. EP0043933B1, 1980.
(20) Frulla, F. F.; Sayigh, A. A. R.; Ulrich, H.; Whitman, P. J., Upjohn Company. Process for preparing di(aminophenyl)methanes. US4039580, 1977.

DOI: 10.1021/cs5017694
ACS Catal. 2015, 5, 734−743

(21) Perego, C.; de Angelis, A.; Farias, O.; Bosetti, A., Enichem S.p.A. Method to produce methylenedianiline and higher homologues. BE1013456A6, 2000.
(22) Clerici, M. G.; Bellussi, G.; Romano, U., Enirichercherche S.p.A. Process for the preparation of 4,4'-diaminodiphenylmethane and its derivatives. EP0264744, 1987.
(23) Perego, C.; de Angelis, A.; Farias, O.; Bosetti, A., Enichem S.p.A. Process for the production of diaminodiphenylmethane and its higher homologues. EP1055663A1, 2000.
(24) Kugita, T.; Hirose, S.; Namba, S. *Catal. Today* **2006**, *111*, 275−279.
(25) Salzinger, M.; Lercher, J. A. *Green Chem.* **2011**, *13*, 149−155.
(26) Corma, A.; Fornes, V.; Pergher, S. B.; Maesen, T. L. M.; Buglass, J. G. *Nature* **1998**, *396*, 353−356.
(27) Corma, A.; Botella, P.; Mitchell, C. *Chem. Commun.* **2004**, 2008−2010.
(28) Botella, P.; Corma, A.; Carr, R. H.; Mitchell, C. J. *Appl. Catal., A* **2011**, *398*, 143−149.
(29) Salzinger, M.; Fichtl, M. B.; Lercher, J. A. *Appl. Catal., A* **2011**, *393*, 189−194.
(30) Verboekend, D.; Vilé, G.; Pérez-Ramírez, J. *Adv. Funct. Mater.* **2012**, *22*, 916−928.
(31) Verboekend, D.; Keller, T. C.; Milina, M.; Mitchell, S.; Pérez-Ramírez, J. *Chem. Mater.* **2013**, *25*, 1947−1959.
(32) Corma, A.; Corell, C.; Pérez-Pariente, J. In *Verified Syntheses of Zeolitic Materials*, 2nd ed.; Robson, H.; Lillerud, K. P., Eds.; Elsevier Science: Amsterdam, 2001; p 225.
(33) Janssen, A. H.; Koster, A. J.; de Jong, K. P. *J. Phys. Chem. B* **2002**, *106*, 11905−11909.
(34) Kortunov, P.; Vasenkov, S.; Kärger, J.; Valiullin, R.; Gottschalk, P.; Fé Elía, M.; Perez, M.; Stöcker, M.; Drescher, B.; McElhiney, G.; Berger, C.; Gläser, R.; Weitkamp, J. *J. Am. Chem. Soc.* **2005**, *127*, 13055−13059.
(35) Milina, M.; Mitchell, S.; Crivelli, P.; Cooke, D.; Pérez-Ramírez, J. *Nat. Commun.* **2014**, *5*, 3922.
(36) Kobayashi, W.; Hara, Y., Tosoh Corp. Method of producing 4,4′-methylenedianiline. JP2012-131721, 2012.

DOI: 10.1021/cs5017694
ACS Catal. 2015, 5, 734−743